Pressure Buildup and Internal Stresses During Binder Burnout: Numerical Analysis

Dah-Shyang Tsai
Dept. of Chemical Engineering, National Taiwan Institute of Technology, Taipei, Taiwan 10772

The interstitial pressure buildup and the internal stresses on the skeleton of a cylindrical green body during burnout are analyzed numerically. The intrinsic kinetics of pyrolysis is coupled with the Carman-Kozeny equation or the slip-flow model of Wakao and Smith to evaluate the pressure distribution. The stress distributions before failure are estimated from elasticity theory. The stresses are tensile, and their maxima are located at the center of the cylinder. The tangential stress is larger than the radial stress. The effects of green body size, specific surface area, and pressurized atmosphere are discussed. The approximate solution is accurate for small green bodies. The pressurized atmosphere reduces the interstitial pressure and the internal stresses effectively.

Introduction

There is a growing awareness of the significance of binder burnout as an essential step in ceramic processing (Rice, 1990; Verweij and Bruggink, 1990; Lewis and Cima, 1990; Cima et al., 1989a; Shukla and Hill, 1989). In the binder burnout step, organic binders, which provide strength and plasticity to ceramic green bodies, are thermally removed before sintering. If the burnout is incomplete, the trapped organic residues will be a contamination source and affect the properties of final product (Masia et al., 1989; Malinowski and Withop, 1978). If the burnout is carried out hastily, defects in green bodies such as spalling, cracking, blisters, and voids, will form, and they cannot be remedied in the later sintering (Dong and Bowen, 1989). Therefore, in order to preserve the quality of the final product the hydrocarbons must be removed slowly, carefully, and completely. On the other hand, shortening burnout time is also desired to decrease operation costs, especially for injection-molded green articles that are fully loaded with organics.

During binder burnout, the organics are heated up thermally, perhaps melted, and decomposed into gases. The evolved gases flow through porous green bodies, then are carried away by a flowing stream. The overall removal is an intricate combination of evaporation, liquid migration, pyrolysis of organics, and heat transfer in porous media. The problem is further compounded by the complexity of the binder recipe (Sheppard, 1990). A general mathematical formulation was given by Stangle and Aksay (1990). In the paper they dealt primarily with the capillary stresses due to the liquid phase and the volume expansion effect due to evaporation. Results of another modeling effort by Calvert and Cima (1990) showed that the formation of pores in the early stages for a heavily loaded tape was a good way to avoid internal bubbles. Unfortunately, the effect of volume expansion from solid to gas due to pyrolysis, which was the major event in burnout, was not taken into consideration in these models. For those green bodies that are not heavily loaded with organics and those injection-molded pieces in which low molecular weight plasticizers are evaporated away and pores are formed, the pressure buildup due to accumulation of decomposed gas is an essential factor in determining the internal stresses.

The pyrolysis of organics with the presence of ceramics is usually studied in an atmosphere-controlled environment using thermal gravimetric analysis (TGA) (Shih et al., 1988; Scheiffele and Sacks, 1988; Sun et al., 1988). Since the amount of sample used in TGA is on the order of a hundred milligram, the kinetic data gathered are considered to represent the intrinsic kinetics of degradation. The temperature distribution in a green body is related to the thermal properties of constitutent phases, the heat effects of pyrolysis, and the convective heat flow due to effluent gas. Although in certain cases the heat effect might be so large that it causes a self-propagating reaction (Verweij et al., 1990), the reaction rate and its accompanying heat generation rate are normally kept low to prevent the sudden generation of a large amount of gas. Similarly, since the gas flow rate is usually small, its convective contribution is also small. The mass flux of evolved gas is

mainly determined by the pore structure and the pressure gradient. The pressure difference between interstitial gas and ambient gas is governed by the degradation rate and the mass transfer rate. Due to this pressure difference, the skeleton of a green body is stressed. These stresses and the mechanical strength of the skeleton decide whether defects or failures will occur.

In this paper a mathematical model is established that combines the intrinsic pyrolysis kinetics, the gas transport in a porous medium, and elasticity theory. This quantitative description provides perspectives for understanding the effects of interstitial pressure and its induced internal stresses in a green body. If the failure criterion is known, this model provides a guide to choose optimal operation variables for a quick and flawless burnout.

Intrinsic Kinetics of Organics Pyrolysis with the Presence of Ceramics

The TGA curves of degradation of many organics follow a single sigmoidal path. Some organics may have two or more sigmoids. Each sigmoid represents a rate-controlling step whose activation energy barrier differs from those of other controlling steps sufficiently. A recipe of the ceramic binder system tailored for the ceramic forming technique often consists of several components. These organic components may be categorized into two groups according to their molecular weights. Low molecular weight organics, such as solvents and plasticizers, are either evaporated away or are decomposed at rather low temperatures. High molecular weight organics, such as binders, possessing higher thermal stability, are pyrolyzed at relatively high temperatures. Consequently the TGA curve often has more than two sigmoids. One sigmoid of this curve could be a superposition of several sigmoids that have similar activation energies. Two sigmoids of this curve could mean two groups of sigmoids with sufficiently separate activation energies. Each sigmoid may be described by three kinetic parameters in an Arrhenius-type equation. These parameters are reaction order n, activation energy E, and frequency factor A. Certain ceramics have catalytic effects on the pyrolysis rate (Masia et al., 1989), however, the shape of the pyrolysis curve with ceramics is similar to that without ceramics. Therefore the mathematical form of organics pyrolysis can still be applied.

The mathematical form that is generally applied to the TGA curve of polymer (Reich and Levi, 1971) is modified to describe the TGA curve of organics pyrolysis with ceramics. In the present analysis we assume that the kinetics is solely controlled by the temperature.

$$-\frac{dW}{dt}=A_1e^{-E_1/RT}\,(W-W_2)^{n_1} + A_2e^{-E_2/RT}\,W^{n_2},\ \text{if } W\geq W_2 \quad (1a)$$

$$-\frac{dW}{dt}=A_2e^{-E_2/RT}W^{n_2},\ \text{if } W<W_2 \quad (1b)$$

W is the mass ratio of organics to ceramic. W_2 is the mass ratio at which degradation moves into the second sigmoidal region. Subscripts 1 and 2 on n, E, and A denote low-temperature and high-temperature degradation, respectively. A decomposition kinetic curve with more than two sigmoids can be expressed in a similar manner.

Temperature and Organic Residues Distribution of a Cylindrical Green Body

A two-step firing cycle consisting of ramping and soaking is assumed. The outer surface temperature of a cylindrical powder compact is raised (ramped) from ambient temperature T_a to soaking temperature T_s, and then is held at the soaking temperature for a period of time. We assume that the pyrolysis rate is so slow that the convective contribution of evolved gas and the heat effect of pyrolysis are negligible. The temperature distribution therefore is dominated by the external heating. The analytical solution of temperature distribution can be found in a classical heat transfer book (Carslaw and Jaeger, 1959).

$$T^*=\frac{t^*}{t_s^*}-\frac{(1-r^{*2})}{4t_s^*}+\frac{2}{t_s^*}\sum_{n=1}^{\infty}e^{-\lambda_n t^*}\,\frac{J_0(r^*\lambda_n^{1/2})}{\lambda_n^{3/2}J_1(\lambda_n^{1/2})},\qquad 0\leq t^*\leq t_s^* \quad (2a)$$

$$T^*=1-\frac{2}{t_s^*}\sum_{n=1}^{\infty}\frac{1}{\lambda_n^{3/2}}\frac{J_0(r^*\lambda_n^{1/2})}{J_1(\lambda_n^{1/2})}\,e^{-\lambda_n(t^*-t_s^*)} + \frac{2}{t_s^*}\sum_{n=1}^{\infty}e^{-\lambda_n t^*}\,\frac{J_0(r^*\lambda_n^{1/2})}{\lambda_n^{3/2}J_1(\lambda_n^{1/2})},\ t_s^*\leq t^* \quad (2b)$$

The dimensionless temperature, radius, and time in Eq. 2 are defined as follows;

- $T^* = (T-T_a)/(T_s-T_a)$, where T is the local temperature
- $r^* = r/R_1$, where R_1 is the radius of the cylinder
- $t^* = \alpha t/R_1^2$, where α is the effective thermal diffusivity
- $t_s^* = \alpha t_s/R_1^2$, where t_s is the ramping time
- λ_n = eigenvalues that satisfy the Bessel function of zero order, $J_0(\lambda_n^{1/2})=0$

Since the intrinsic kinetics of decomposition and the temperature distribution in green bodies are known, the organic residue distribution along radial position at each time interval can be solved numerically.

Interstitial Pressure in a Cylindrical Green Body

An equation of continuity can be written for the gas phase within a green body:

$$\frac{\partial(e\rho_g)}{\partial t}=-\left(\frac{1}{r}\frac{\partial}{\partial r}(r\rho_g v)\right)-\rho_c V_c\frac{\partial W}{\partial t} \quad (3)$$

ρ_g, ρ_c are the densities of gas and ceramic respectively; e is the porosity; v is the superficial velocity of gas flow averaged over a region of space that is small with respect to macroscopic dimensions in the green body but large with respect to the pore size. $-\rho_c V_c\,(\partial W/\partial t)$ represents the mass decrease of organics due to degradation, which also is the mass increase in the gas phase. Since the dimensional change of the cylinder during burnout is often negligible and the volume fraction of ceramic, V_c, is constant, the sum of binder volume fraction V_b and porosity e is constant:

$$V_b+e=1-V_c=\text{constant}$$

The change of porosity is related to the change of binder concentration.

$$\frac{\partial e}{\partial t} = -\frac{\partial V_b}{\partial t} = -\frac{\rho_c V_c}{\rho_b}\frac{\partial W}{\partial t} \tag{4}$$

The first term in Eq. 3 can be rearranged as follows,

$$\frac{\partial (e\rho_g)}{\partial t} = e\frac{\partial \rho_g}{\partial t} - \rho_g \left(\frac{\rho_c}{\rho_b}\right) V_c \frac{\partial W}{\partial t} \tag{5}$$

If the particles of green bodies are loosely packed, the average pore radius is rather large compared with the mean free path of gas, the flow through the powder compact can be regarded as laminar or Poiseuille flow. The Carman-Kozeny model is applied to relate the superficial velocity with the pressure gradient:

$$v = -\frac{e^3}{K_0 S_0^2}\frac{1}{\mu}\frac{\partial P}{\partial r} \tag{6}$$

The best value of K_0 to fit most experimental data on packed beds is equal to 5 (Dullien, 1979). S_0 is the surface area per unit volume green body. μ is the viscosity of gas. If the interstitial gas obeys the ideal gas law, the density of gas in Eqs. 3 and 5 can be rewritten as a function of pressure and temperature. By substituting Eqs. 5 and 6 into Eq. 3 and rearranging, a partial differential equation of pressure in dimensionless form is obtained:

$$\frac{\partial P^*}{\partial t^*} = \frac{K_1}{K_0}\frac{(T^* + T_a^*)}{e}\left[\frac{1}{r^*}\frac{\partial}{\partial r^*}\left(r^*\frac{e^3 P^*}{(T^* + T_a^*)}\frac{\partial P^*}{\partial r^*}\right)\right] + \frac{P^*}{(T^* + T_a^*)}\frac{\partial T^*}{\partial t^*} + \left[\left(\frac{\rho_c}{\rho_b}\right) V_c \left(\frac{P^*}{e}\right) - \frac{\rho_c V_c}{\rho_{g0}}\frac{(T^* + T_a^*)}{e}\right]\frac{\partial W}{\partial t^*} \tag{7}$$

in which $\rho_{g0} = P_0 M/R(T_s - T_a)$, P_0 is the ambient pressure, M is the average molecular weight of evolved gas, R is the gas constant, $T_a^* = T_a/(T_s - T_a)$, $P^* = P/P_0$, and $K_1 = P_0/S_0^2\mu\alpha$.

If the average radius of capillaries in a green body is much smaller than the mean free path, gas transport occurs by Knudsen flow (Knudsen, 1909). Slip flow occurs when the gas transport is intermediate between laminar flow and Knudsen flow, a range of 0.1 to 10 a/λ_g, where a and λ_g are respectively the average pore radius and the mean free path (Scott et al., 1962). Since the mean free paths of gases are, under room temperatures and ordinary pressures, roughly in the range of 100 to 1,000 Å, it can be shown that in an alumina powder compact with green density equal to 60% theoretical density ($V_c = 0.6$), and BET surface area equal to 5 m^2/g, the average pore radius a is equal to 669 Å, which is in the slip flow range. The average pore radius is estimated from the equation, $a = 2e/S_0$. Since the trend in fine ceramics is toward using submicron powders and densely packed green bodies, this simple calculation reveals that flows in many green bodies should be in the transient range. For a single capillary, the molar flux of gas flow N in the transient region is derived by Wakao et al. (1965); Otani et al. (1965):

$$N = -\frac{K}{RT}\frac{\partial P}{\partial r}$$

where

$$K = \frac{\frac{2}{3}a\left(\frac{8RT}{\pi M}\right)^{1/2}}{1 + 2a/\lambda_g} + \frac{1}{1 + \lambda_g/2a}\left[\frac{\pi a}{6}\left(\frac{8RT}{\pi M}\right)^{1/2} + \frac{a^2 P}{8\mu}\right] \tag{8}$$

The mean free path of gas is estimated by the equation $\lambda_g = 1/2^{1/2}\pi d^2 n$, where d is the diameter of gas molecules—a typical value is 4 Å—and n is the number of gas molecules per unit volume that can be calculated from the ideal gas law. The local mass flux in a green body is the product of mass flux of a single capillary and the local pore volume fraction e:

$$\rho_g v = NMe \tag{9}$$

By substituting Eqs. 9 and 8 into Eq. 3, a similar governing equation of pressure based on the transient flow model is obtained. This equation is written in a dimensionless form as follows,

$$\frac{\partial P^*}{\partial t^*} = \frac{(T^* + T_a^*)}{e}\left\{\frac{1}{r^*}\frac{\partial}{\partial r^*}\left[r^*\frac{(K/\alpha)e}{(T^* + T_a^*)}\frac{\partial P^*}{\partial r^*}\right]\right\} + \frac{P^*}{(T^* + T_a^*)}\frac{\partial T^*}{\partial t^*} + \left[\left(\frac{\rho_c}{\rho_b}\right) V_c \left(\frac{P^*}{e}\right) - \frac{\rho_c V_c}{\rho_{g0}}\frac{(T^* + T_a^*)}{e}\right]\frac{\partial W}{\partial t^*} \tag{10}$$

where

$$(K/\alpha)e = \left[\frac{4}{3}K_3 e^2 (T^* + T_a^*)^{3/2} + \frac{4}{3}\pi K_3 K_4 e^3 P^* (T^* + T_a^*)^{1/2} + \frac{2K_4 K_1 e^4 P^{*2}}{[4K_4 eP^* + T^* + T_a^*]}\right]$$

$$K_3 = \frac{[8R(T_s - T_a)/\pi M]^{1/2}}{(S_0\alpha)}$$

$$K_4 = \frac{2^{1/2}\pi d^2 N_0 P_0}{S_0 R(T_s - T_a)}$$

Under the assumptions of pseudosteady state $[\partial(e\rho_g)/\partial t = 0]$, uniform temperature, and uniform removal of organics, the pressure distribution can be reduced to simpler forms.

For the Carman-Kozeny equation:

$$P^* = \left[1 + \frac{\xi}{\nu}\left(1 - r^{*2}\right)\right]^{1/2}$$
$$\xi = \frac{K_0}{K_1}\frac{1}{e^3}\frac{\rho_c V_c}{\rho_{g0}}(T^* + T_a^*)\left(-\frac{\partial W}{\partial t^*}\right) \tag{11}$$

For slip flow:

$$\frac{K_1 e^2 (P^*-1)[2K_4 e(P^*+1)-(T^*+T_a^*)]}{8K_4}+\frac{\pi}{3}K_3 e^2 (T^*+T_a^*)^{1/2}(P^*-1)$$
$$+\frac{3K_1 e(T^*+T_a^*)^2-8\pi K_3 K_4 e(T^*+T_a^*)^{3/2}+32K_3 K_4 e(T^*+T_a^*)^{3/2}}{96K_4^2}\ln\left[\frac{4K_4 eP^*+T^*+T_a^*}{4K_4 e+T^*+T_a^*}\right]$$
$$=\frac{\rho_c V_c}{\rho_{g0}}(T^*+T_a^*)\left(-\frac{\partial W}{\partial t^*}\right)\left[\frac{1-r^{*2}}{2\nu}\right] \quad (12)$$

Similar equations for planar and spherical geometries are also derived. In Eqs. 11 and 12 ν is 1 for slab, 2 for cylinder, 3 for sphere.

Internal Stresses on the Skeleton

Because of the inherent axial symmetry of the concentric shell, stress, strain, and displacement fields are independent of the polar angle θ. We neglect the body force, and assume that the distance between two plane cross sections of the shell normal to the z axis remains constant—the assumption of plane strain. Therefore, only radial displacement exists. We further assume that the mechanical properties of the skeleton do not change during burnout and the deformation of the skeleton is so small that it will not affect the gas flow and the heat transfer described earlier. Under the equilibrium condition,

$$\frac{\partial(r\sigma_r)}{\partial r}-\sigma_\theta=0 \quad (13)$$

Both the radial and the tangential stresses, σ_r, σ_θ, consist of contributions from the gas phase and the solid phase (skeleton). The sign convention is taken as positive for tension, negative for compression:

$$\sigma_r=-P+\sigma_{rs} \quad (14a)$$

$$\sigma_\theta=-P+\sigma_{\theta s} \quad (14b)$$

The stresses, σ_{rs}, $\sigma_{\theta s}$, strains, ϵ_{rs}, $\epsilon_{\theta s}$, and displacement, u_{rs}, of the skeleton bear the following relations:

$$\sigma_{rs}=(\lambda+2G)\epsilon_{rs}+\lambda\epsilon_{\theta s} \quad (15a)$$

$$\sigma_{\theta s}=(\lambda+2G)\epsilon_{\theta s}+\lambda\epsilon_{rs} \quad (15b)$$

$$\epsilon_{rs}=\partial u_{rs}/\partial r \quad (15c)$$

$$\epsilon_{\theta s}=u_{rs}/r \quad (15d)$$

where λ and G are two Lame's constants of the skeleton, λ is Lame's elastic constant, and G is the modulus of rigidity (Jumikis, 1969). Substituting Eqs. 15a, b, c, d and Eqs. 14a, b into Eq. 13, we obtain an ordinary differential equation for displacement in dimensionless form:

$$\frac{d^2u_{rs}^*}{dr^{*2}}+\frac{1}{r^*}\frac{du_{rs}^*}{dr^*}-\frac{1}{r^{*2}}u_{rs}^*=\zeta\left(\frac{\partial P^*}{\partial r^*}\right) \quad (16)$$

where $\zeta=1/(\lambda^*+2G^*)$, subject to $u_{rs}^*=0$ at $r^*=0$ and $(\lambda^*+2G^*)(du_{rs}^*/dr^*)+\lambda^* u_{rs}^*=0$ at $r^*=1$.

In Eq. 16, $u_{rs}^*=u_{rs}^*/R_1$; $\lambda^*=\lambda/P_0$; $G^*=G/P_0$. If the pressure gradient is known, the displacement and the stresses can be solved. The approximate displacement of laminar flow in analytical form can be obtained by substituting Eq. 11 into Eq. 16. The approximate strains and the approximate stresses are obtained by substituting the displacement into Eq. 15a, b, c, d. The analytical result is given in the appendix. When the gas evolution approaches zero, $\xi->0$, the displacement of Eq. A1, the strains of Eqs. A2, A3, and the stresses of Eqs. A4, A5 are reduced to the values under unstressed conditions:

$$u_{rs}^*=\epsilon_{rs}=\epsilon_{\theta s}=\sigma_{rs}^*=\sigma_{\theta s}^*=0 \quad (17)$$

Eqs. 17 are the trivial solution of Eq. 16 with $\zeta(\partial P^*/\partial r^*)$ equal to zero.

Numerical Methods

The infinite series in Eq. 2a converges poorly when time t^* is smaller than 0.02. To ensure the accuracy of the initial temperature, a small time expansion has to be done. Similar to the treatment of Carslaw and Jaeger (1959), the Bessel function, Eq. 2a, is expanded asymptotically to obtain a form involving an exponential function containing $(1/t^*)$. This form converges much quicker for small time provided that r^* is not too small.

The orthogonal collocation method is applied to solve the nonlinear partial differential equations of Eq. 7 and Eq. 10, and the ordinary differential equation of Eq. 16. Since the pressure distribution is symmetric about $r^*=0$, orthogonal polynomials of r^{*2} with weighting function $(1-r^{*2})$ are constructed for the pressure. The boundary condition at $r^*=0$ is automatically satisfied. On the other hand, the displacement distribution is not symmetric about $r^*=0$. Unsymmetric polynomials with weighting function 1 are constructed. The chosen collocation points that are roots to unsymmetric polynomials, including 0 and 1, are listed in Table 2. The collocation method and the selection of collocation points are thoroughly discussed by Finlayson (1980). In solving Eq. 16, $\partial P^*/\partial r^*$ is interpolated from the known pressure distribution at each time interval. These initial-value problems of residues and pressure at collocation points are solved by the RKF45D package (Forsythe et al., 1977).

Burnout Conditions and Physical Properties

The properties of a green body and its pyrolysis rate con-

Table 1. Burnout Conditions, Physical Constants of Green Bodies, and Pyrolysis Rate Constants

Soaking temp., $T_s = 773$ K
Ambient temp., $T_a = 293$ K
Ramping time, $t_s = 5$ h

Ceramic density (alumina) $\rho_c = 3.987 \times 10^3$ kg/m^3
Binder density, $\rho_b = 1.25 \times 10^3$ kg/m^3
Vol. frac. of ceramic, $V_c = 0.6$
Init. organics loading, $W = 0.08$ ($W_2 = 0.05$)

Eff. thermal diffusivity, $\alpha = 1.015 \times 10^{-7}$ m^2/s
Evolved gas viscosity $\mu = 2.50 \times 10^{-2}$ m Pa•s
Mole. wt. of evolved gas, $M = 30$

Order of reaction n_1, n_2 = 2.0, 3.0
Frequency factor A_1, A_2 = 8×10^{23}, 4×10^{28} min^{-1}
Activation energy/gas constant
$E_1/R = 2.45 \times 10^4$ K
$E_2/R = 3.6 \times 10^4$ K
Lame constant λ, $G = 116.9 \times 10^5$, 77.9×10^5 N/m^2

	Case A	Case B	Case C	Case D
Radius, cm	5	5	1	5
Amb. press., atm	1	1	1	10
Spec. surf. area, cm^{-1}	11.961×10^4	1.6745×10^4	11.961×10^4	11.961×10^4
K_1	279.124	14,241.0	279.124	2,791.24
K_3	479.407	–	479.407	479.407
K_4	0.90844	–	0.90844	9.0844

stants are listed in Table 1. The effective thermal conductivity is estimated from the Hashin-Strikman (1962) lower bound for two-phase materials. The slip-flow model is applied to cases A, C, and D, which have high specific surface areas. The Carman-Kozeny equation is applied to case B, where surface area is relatively low.

Results and Discussion

Whether a failure or a defect will occur is determined by the local strength of the skeleton and the local stresses on the skeleton. The major purpose of the above modeling effort is to provide a quantitative estimate of the latter. The stresses are influenced by many factors, such as initial organics loading, temperature profile of the furnace, and pyrolysis characteristics, to name only a few. In this paper three factors are emphasized that are rarely discussed in the literature: the green body size, the specific surface area, and the pressurized atmosphere.

Table 2. Collocation Points of Orthogonal Collocation Method with Weight Function 1

	r_i^*	r_i^*
1	0.00000000	0.00000000
2	0.01088567	0.04691008
3	0.05646870	0.23076534
4	0.13492400	0.50000000
5	0.24045194	0.76923466
6	0.36522842	0.95308992
7	0.50000000	1.00000000
8	0.63477158	—
9	0.75954806	—
10	0.86507600	—
11	0.94353130	—
12	0.98911433	—
13	1.00000000	—

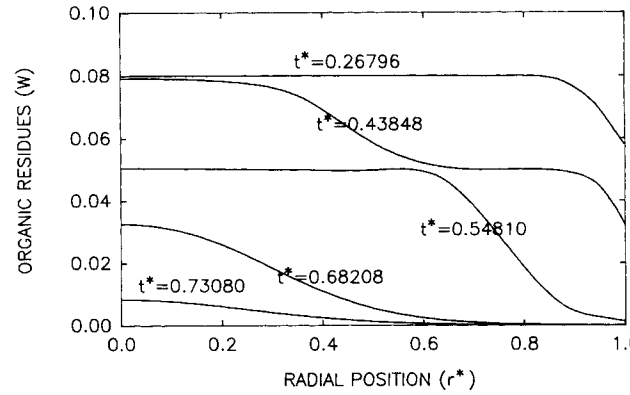

Figure 1. Organic residues vs. radial position, cases A, B, D during burnout.

Figure 1 shows the organic residues distribution of cases A, B, and D in the ramping stage during burnout. Since the surface temperature is higher than the core temperature, the surface organics start to decompose first, at $t^* = 0.26796$. Also, due to a rather large radius, at $t^* = 0.43848$ (3 h) there is a temperature difference $\Delta T^* = 0.3121$ (149.8°C) between $r^* = 1$ and $r^* = 0$. Accordingly, when the organics at the surface are proceeding with the second sigmoidal pyrolysis ($W = 0.03226$ at $r^* = 1$), the organics at core just begin the first sigmodal pyrolysis ($W = 0.07921$ at $r^* = 0$). At the end of the ramping stage ($t^* = 0.7308$), there is still some amount of organics remaining, $W = 0.00835$ at $r^* = 0$. For a cylinder of smaller radius, case C, there is much less temperature difference ($\Delta T^* = 0.0137$, 6.6°C) and less residues difference ($\Delta W = 0.00639$) between surface and core at $t^* = 10.962$ (3 h). Also, much less organics at $r^* = 0$ remain at the end of the ramping stage ($W = 0.0000179$ at $t^* = 18.27$).

For the organics decomposed at the surface ($r^* = 1$), the evolved gas easily escapes the porous body. Nevertheless, the exit of gas evolved within the green body ($r^* < 1$) needs the establishment of a pressure gradient. Therefore a region of high evolution rate of gas is accompanied with a steep pressure gradient. The pressure gradients of cases A and B at $t^* = 0.43848$ represent a typical example, as shown in Figure 2. In the region near the core ($r^* = 0.0$–0.2), organics decompose only a little, the pressure gradient is close to zero. In the region between $r^* = 0.4$ and 0.6 the gas evolution rate is high and its corresponding pressure gradient is steep. In the surface region ($r^* = 0.95$–1.0) the pressure gradient drops further because the surface region undergoes the second sigmoidal decomposition. For both cases the pressure buildup in the core region indicates an accumulation of gas. This accumulated gas is originated from the region $r^* > 0.2$ because only a little of the core region organics ($r^* < 0.2$) is burnt. The radial and tangential stresses on the skeleton at $t^* = 0.43848$ are also plotted in Figure 2. Initially the skeleton of green body is under the unstressed condition, σ_{rs}^*, $\sigma_{\theta s}^* = 0$. The interstitial pressure difference between surface and core exerts force on the skeleton of the green body in the positive r direction. For a 5 cm radius cylinder, case A, a pressure difference ΔP^* of 3.144 causes tensile stresses $\sigma_{rs}^* = \sigma_{\theta s}^* = 2.668$ at $r^* = 0$. For a larger average pore size, case B, the pressure difference is less, $\Delta P^* = 1.402$, and so are the tensile stresses, $\sigma_{rs}^* = \sigma_{\theta s}^* = 1.212$ at $r^* = 0$. For both cases the radial stresses are zero at $r^* = 1$. The tangential stress at $r^* = 1$ is $\sigma_{\theta s}^* = 0.845$ for A, 0.421 for B.

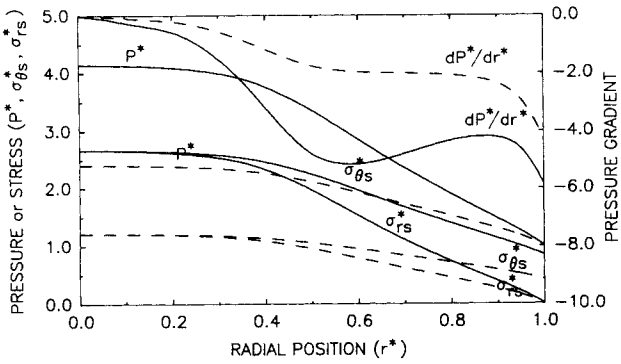

Figure 2. Interstitial pressure, pressure gradient, radial stress, and tangential stress, cases A, B at $t^* = 0.43848$.

——— case A; – – – case B

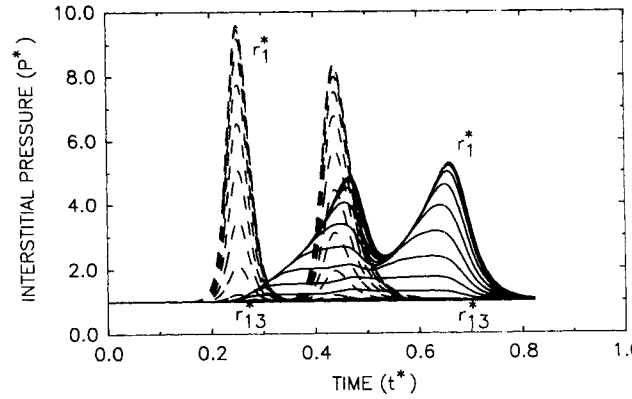

Figure 4. Solutions of interstitial pressure at thirteen collocation points, case A.

——— numerical solution; – – – approx. solution

Therefore, a higher pressure difference causes a higher tangential stress at the surface.

Figures 3a and 3b show the residues variation with time at collocation points for a 5 cm (thirteen points) and a 1 cm (seven points) radius cylinder, respectively. The removal of organics in the 5 cm radius cylinder is spread in a much wider time domain.

The interstitial pressure variation with time at thirteen collocation points of case A is illustrated in Figure 4. As the evolved gas starts to accumulate in the green body, the pressure begins to rise. Pressures of points near the core, such as r^*_1, r^*_2, r^*_3, r^*_4, exhibit two peak values, which are the characteristics of pyrolysis. The peak value of each collocation point decreases and shifts forward progressively as its position shifts away from the center. Pressures of collocation points near surface, such as r^*_{10}, r^*_{11}, r^*_{12}, start to increase due to the decomposition of their own organics. However these pressures do not drop after the degradation of their organics is completed. It is the decomposition of inner organics and the accumulated pressure inside that sustains these pressures near the surface at those levels. The approximate solution of pressure is also shown in Figure 4. It represents the pressure generated by uniform removal of organics in the green body. It may serve as the upper limit of the prediction. Since the organics at every location are assumed to be burnt simultaneously, the two pressure peaks are clearly separated in the approximate solution. Figure 4 demonstrates that for a large piece of green body the approximate solution provides a poor result. Figure 5 is the radial stress on the skeleton of case A and its approximate solution. The variation of radial stress with time resembles that of pressure. The tangential stress of case A is shown in Figure 6. The tangential stresses of the surface region are significantly higher than the corresponding radial stresses. When the interstitial pressure is at its maxima, so are the stresses in both directions.

Figure 7 shows the pressure of 1 cm radius green body, case C, at seven collocation points. The accumulated pressure and the stresses are lower in case C due to the smaller radius. Since organics removal is nearly uniform in the green body, as shown in Figure 3(b), the approximate pressure and the numerical solution are very close. The approximate stresses are even closer to the numerical result. The case of a 1 cm radius green body with specific surface area equal to case B is also computed. Its result is very similar to that of case C. Therefore, it shows that under a fixed ramping rate of furnace temperature the pressure buildup and internal stresses of small green bodies can be predicted by the approximate solutions, Eqs. 11, 12, A4, and A5.

The effect of pressurized atmosphere is illustrated in Figure 8. Pressures and stresses of the green body under 1 atm, case A, and under 10 atm, case D, are plotted against r^* when pressures and stresses are at their maximum values at $t^* = 0.65772$. The pressure difference between surface and core of case A is $\Delta P^* = 4.268 = 4.268$ atm; on the other hand, the

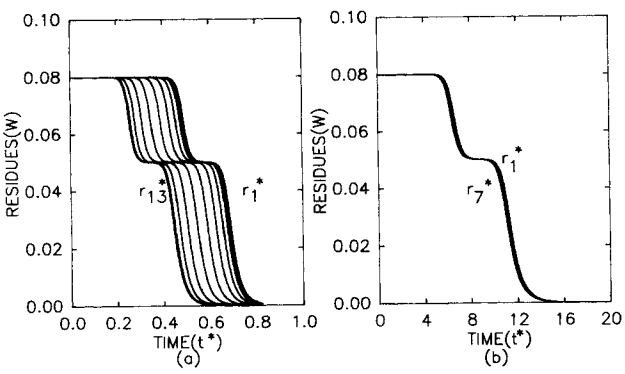

Figure 3. Organic residues vs. time at collocation points.

a. 5 cm radius green body

b. 1 cm radius green body.

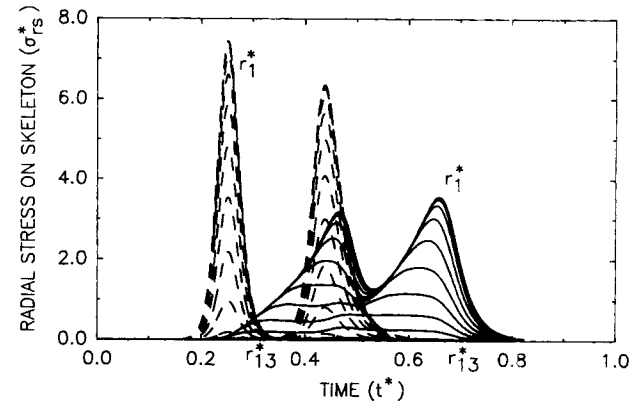

Figure 5. Solutions of radial stress on skeleton at thirteen collocation points, case A.

——— numerical solution; – – – approx. solution

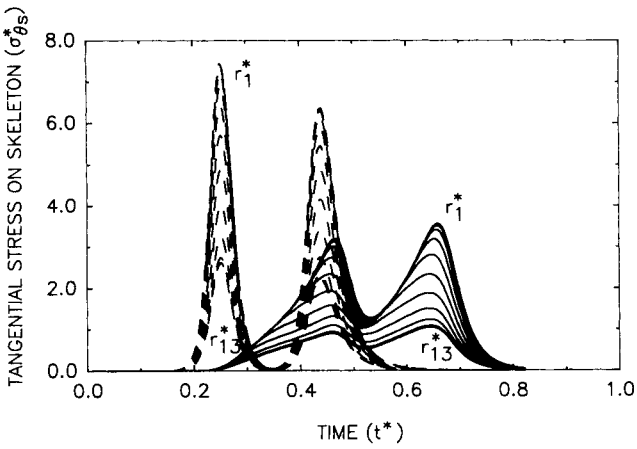

Figure 6. Solutions of tangential stress on skeleton at thirteen collocation points, case A.

——— numerical solution; – – – approx. solution

corresponding pressure difference of case D is $\Delta P^* = 0.285 = 2.85$ atm. Also the tensile stresses are effectively reduced by the pressurization. The tangential stress at the surface is reduced from $\sigma^*_{\theta s} = 1.022 = 1.022$ atm to $\sigma^*_{\theta s} = 0.0673 = 0.673$ atm, as shown in Figure 8. This reduction of pressure buildup and the tensile stresses indicates that pressurization is a useful technique in preventing defects, as is shown in two patents (Sakai et al., 1985, Wiech, 1981).

The tangential and the radial stresses are both tensile in the four examples presented. Since the powder compact is much more vulnerable against tension rather than compression (Stangle and Aksay, 1990), the effect of pressure buildup is important in designing a safe burnout operation. Another interesting point is that the tangential stress is larger than the radial stress at the surface. This result implies that if a crack is initiated from a surface flaw, the crack will propagate inward.

Conclusions

A numerical analysis was performed to estimate the residues, interstitial pressure, and internal stress distributions in a cylindrical green body during burnout. Pressures and stresses of small-radius green bodies can be closely evaluated by simplified

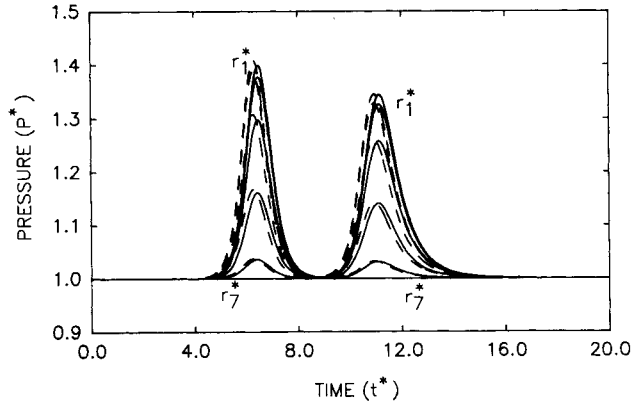

Figure 7. Solutions of interstitial pressure at seven collocation points, case C.

——— numerical solution; – – – approx. solution

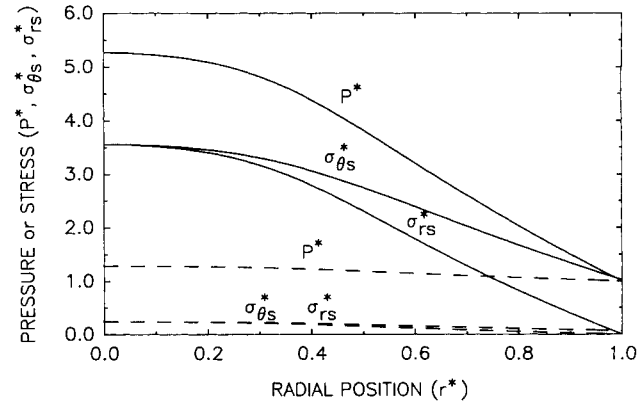

Figure 8. Interstitial pressure, radial stress, and tangential stress on skeleton, cases A, D at $t^* = 0.65772$.

——— case A; – – – case D

equations obtained under the assumption of uniform removal of organics. These approximate solutions deviate considerably from the numerical solutions for large-radius green bodies. For a green body of low surface area, the interstitial pressure and the stresses on the skeleton are less because of larger pore size. For a green body under pressurized atmosphere, the pressure buildup and the tension on the skeleton both decrease.

Acknowledgment

We thank the computer center of the Ministry of Education for free computation time. We are also grateful to Prof. M. K. Kuo and Y. S. Chou for constructive opinions, as well as to Prof. Sundaresan for his help in formulating the stress equations correctly.

Notation

A_1, A_2 = frequency factor of pyrolysis reaction, s^{-1}
a = average pore radius, m
d = diameter of gas molecule, m
E_1, E_2 = activation energy of pyrolysis reaction, kJ/kmol
e = porosity
G = modulus of rigidity of skeleton, N/m^2
K, K_0, K_1, K_3, K_4 = constants, Eqs. 7, 8, 10
M = molecular weight of evolved gas, kg/kmol
n = number of gas molecules per unit volume, m^{-3}
n_1, n_2 = order of decomposition reaction
N = molar flux of evolved gas, $kmol/m^2$
N_0 = Avogadro's number
P, P_0 = gas pressure, ambient pressure, N/m^2
r = radial position, m
R = gas constant, kJ/kmol·K
R_1 = radius of cylinder, m
S_0 = surface area per unit volume, m^{-1}
t, t_s = time, ramping time of furnace, s
T, T_a, T_s = temperature, ambient temperature, soaking temperature, K
u_{rs} = displacement of skeleton in radial direction, m
v = superficial velocity of evolved gas, m/s
V_b, V_c = volume fraction of binder, ceramic
W = mass of organic residues/mass of ceramics

Greek letters

α = effective thermal diffusivity, m^2/s
$\epsilon_{rs}, \epsilon_{\theta s}$ = radial and tangential strain of skeleton
λ = Lame's elastic constant of skeleton, N/m^2
λ_g = mean free path of gas, m
λ_n = eigenvalues that satisfy $J_0(\lambda_n^{1/2}) = 0$

μ = gas viscosity, N·s/m^2
ν = shape factor, 1 for slab, 2 for cylinder, 3 for sphere
ρ_b, ρ_c, ρ_g = density of binder, ceramic, gas, kg/m^3
ρ_{g0} = pseudo gas density, Eq. 7, kg/m^3
σ_r, σ_θ = radial, tangential stress, N/m^2
σ_{rs}, $\sigma_{\theta s}$ = radial, tangential stress on skeleton, N/m^2
ξ = constant, Eq. 11
ζ = constant, Eq. 16

Superscript

* = dimensionless

Literature Cited

Calvert, P., and M. Cima, "Theoretical Models for Binder Burnout," *J. Am. Ceram. Soc.*, **73**, 575 (1990).

Carslaw, H. S., and J. C. Jaeger, *Conduction of Heat in Solids*, Clarendon, Oxford, 201, 330 (1959).

Cima, M. J., J. A. Lewis, and A. D. Devoe, "Binder Distribution in Ceramic Greenware During Thermolysis," *J. Am. Ceram. Soc.*, **72**, 1192 (1989a).

Cima, M. J., M. Dudziak, and J. A. Lewis, "Observation of Polyvinyl Butyral-Dibutyl Phthalate Binder Capillary Migration," *J. Am. Ceram. Soc.*, **72**, 1087 (1989b).

Dong, C., and H. K. Bowen, "Hot-Stage Study of Bubble Formation During Binder Burnout," *J. Am. Ceram. Soc.*, **72**, 1082 (1989).

Dullien, F. A. L., *Porous Media Fluid Transport and Pore Structure*, Academic Press, New York, 171 (1979).

Finlayson, B. A., *Nonlinear Analysis in Chemical Engineering*, McGraw-Hill, New York, 73-97 (1980).

Forsythe, G. E., M. A. Malcolm, and C. B. Moler, *Computer Methods for Mathematical Computations*, Prentice-Hall, Englewood Cliffs, NJ, 129-147 (1977).

Hashin, Z., and S. Strikman, "A Variational Approach to the Theory of the Effective Magnetic Permeability of Multiphase Materials," *J. Appl. Phys.*, **33**, 3125 (1962).

Jumikis, A. R., *Theoretical Soil Mechanics*, Van Nostrand, New York, 42-43 (1969).

Knudsen, M., *Annalen der Physik*, **28**, 75 (1909).

Lewis, J. A., and M. J. Cima, "Diffusivities of Dialkyl Phthalates in Plasticized Poly(Vinyl Butyral): Impact on Binder Thermolysis," *J. Am. Ceram. Soc.*, **73**, 2702 (1990).

Malinowski, W., and A. Withop, "Organic Sources of Voids in Ceramics," *Ceram. Bull.*, **57**, 523 (1978).

Masia, S., P. D. Calvert, W. E. Rhine, and H. K. Bowen, "Effect of Oxides on Binder Burnout During Ceramics Processing," *J. Mater. Sci.*, **24**, 1907 (1989).

Otani, S., N. Wakao, and J. M. Smith, "II: Diffusion and Flow in Porous Catalysts," *AIChE J.*, **11**, 439 (1965).

Reich, L. R., and D. W. Levi, "Thermogravimetric Analysis," *Encyc. Polymer Sci. and Technol.*, **14**, N. M. Bikales, ed., McGraw-Hill, New York (1971).

Rice, R. W., "Ceramic Processing: An Overview," *AIChE J.*, **36**, 481 (1990).

Sakai, T., M. Inoue, Y. Kihara, and Y. Kawabata, "Debindering Method for Ceramic Green Moldings," Japan Pat. No. 215578 456-7 (1985).

Scheiffele, G. W., and M. D. Sacks, "Pyrolysis of Polyvinyl Butyral Binders: II. Effects of Processing Variables," *Ceram. Trans.*, **1**, A 559, Ceramic Powder Science, Am. Ceram. Soc. (1988).

Scott, D. S., and F. A. L. Dullien, "Diffusion of Ideal Gases in Capillaries and Porous Solids," *AIChE J.*, **8**, 113 (1962).

Scott, D. S., and F. A. L. Dullien, "The Flow of Rarefied Gases," *AIChE J.*, **8**, 293 (1962).

Sheppard, L. M., "The Changing Demand for Ceramic Additives," *Ceram. Bull.*, **69**, 802 (1990).

Shih, W. K., M. D. Sacks, G. W. Scheiffele, Y. N. Sun, and J. W. Williams, "Pyrolysis of Polyvinyl Butyral Binders. I: Degradation Mechanisms," 549, *Ceram. Trans.*, **1**, A, 549, Ceramic Powder Science, Am. Ceram. Soc. (1988).

Shukla, V. N. and D. C. Hill, "Binder Evolution from Powder Compacts: Thermal Profile for Injection-Molded Articles," *J. Am. Ceram. Soc.*, **72**, 1797 (1989).

Stangle, G. C., and I. A. Aksay, "Simultaneous Momentum, Heat and Mass Transfer with Chemical Reaction in a Disordered Porous Medium: Application to Binder Removal from a Ceramic Green Body," *Chem. Eng. Sci.*, **45**, 1719 (1990).

Sun, Y. N., M. D. Sacks, and J. W. Williams, "Pyrolysis Behavior of Acrylic Polymers and Acrylic Polymer/Ceramic Mixtures," *Ceram. Trans.*, **1**, A, 538, Ceramic Powder Science, Am. Ceram. Soc. (1988).

Verweij, H., and W. H. M. Bruggink, "Reaction-Controlled Binder Burnout of Ceramic Multilayer Capacitors," *J. Am. Ceram. Soc.*, **73**, 226 (1990).

Wakao, N., S. Otani, and J. M. Smith, "Significance of Pressure Gradients in Porous Materials. I: Diffusion and Flow in Fine Capillaries," *AIChE J.*, **11**, 435 (1965).

Wiech, R. E., "Methods and Means for Removing Binder from a Green Body," Eur. Pat. No. 0032404 (1981).

Appendix

For the pressure distribution of Eq. 11, analytical solutions for displacement, strains, and stresses are possible.

$$u_{rs}^* = \left\{ -\frac{1}{2(\lambda^* + G^*)} - \frac{2}{3}\frac{G^*}{(\lambda^* + G^*)}\frac{\zeta}{\xi}\left[1 - \left(1 + \frac{\xi}{2}\right)^{3/2}\right]\right\} r^* - \frac{2}{3}\frac{\zeta}{\xi}\frac{1}{r^*}\left[\left(1 + \frac{\xi}{2} - \frac{\xi}{2}r^{*2}\right)^{3/2} - \left(1 + \frac{\xi}{2}\right)^{3/2}\right] \quad \text{(A1)}$$

$$\epsilon_{rs} = \left\{ -\frac{1}{2(\lambda^* + G^*)} - \frac{2}{3}\frac{G^*}{(\lambda^* + G^*)}\frac{\zeta}{\xi}\left[1 - \left(1 + \frac{\xi}{2}\right)^{3/2}\right]\right\} + \zeta\left(1 + \frac{\xi}{2} - \frac{\xi}{2}r^{*2}\right)^{1/2} + \frac{2}{3}\frac{\zeta}{\xi}\frac{1}{r^{*2}}\left[\left(1 + \frac{\xi}{2} - \frac{\xi}{2}r^{*2}\right)^{3/2} - \left(1 + \frac{\xi}{2}\right)^{3/2}\right] \quad \text{(A2)}$$

$$\epsilon_{\theta s} = \left\{ -\frac{1}{2(\lambda^* + G^*)} - \frac{2}{3}\frac{G^*}{(\lambda^* + G^*)}\frac{\zeta}{\xi}\left[1 - \left(1 + \frac{\xi}{2}\right)^{3/2}\right]\right\} - \frac{2}{3}\frac{\zeta}{\xi}\frac{1}{r^{*2}}\left[\left(1 + \frac{\xi}{2} - \frac{\xi}{2}r^{*2}\right)^{3/2} - \left(1 + \frac{\xi}{2}\right)^{3/2}\right] \quad \text{(A3)}$$

$$\sigma_{rs}^* = -1 - \frac{4}{3}G^*\frac{\zeta}{\xi}\left[1 - \left(1 + \frac{\xi}{2}\right)^{3/2}\right] + \left(1 + \frac{\xi}{2} - \frac{\xi}{2}r^{*2}\right)^{1/2} + \frac{4}{3}G^*\frac{\zeta}{\xi}\frac{1}{r^{*2}}\left[\left(1 + \frac{\xi}{2} - \frac{\xi}{2}r^{*2}\right)^{3/2} - \left(1 + \frac{\xi}{2}\right)^{3/2}\right] \quad \text{(A4)}$$

$$\sigma_{\theta s}^* = -1 - \frac{4}{3}G^*\frac{\zeta}{\xi}\left[1 - \left(1 + \frac{\xi}{2}\right)^{3/2}\right] + \lambda^*\zeta\left(1 + \frac{\xi}{2} - \frac{\xi}{2}r^{*2}\right)^{1/2} - \frac{4}{3}G^*\frac{\zeta}{\xi}\frac{1}{r^{*2}}\left[\left(1 + \frac{\xi}{2} - \frac{\xi}{2}r^{*2}\right)^{3/2} - \left(1 + \frac{\xi}{2}\right)^{3/2}\right] \quad \text{(A5)}$$

Manuscript received Oct. 10, 1990, and revision received Jan. 18, 1991.